Novel Polyaniline/Titanium Nitride Nanocomposite: Controllable Structures and Electrical/Electrochemical Properties

Yu Qiu and Lian Gao*

State Key Laboratory of High Performance Ceramics and Superfine Microstructure, Shanghai Institute of Ceramics, Chinese Academy of Sciences, Shanghai 200050, P.R. China.

Received: July 13, 2005

We first present the preparation of a new class of polyaniline (PANI)/titanium nitride (TiN) nanocomposites by in situ chemical polymerization in the presence of TiN nanoparticles. It was found that nanocrystalline TiN with an average diameter of ∼20 nm incorporated and dispersed homogeneously within the polymer matrix, leading to enhanced conductivity and electrochemical activity. The interaction between nanocrystalline TiN and the polymer matrix was characterizd by XRD, FTIR, and UV−vis spectra. Interestingly, the morphology and structure of the PANI/TiN were controlled by the content of TiN nanoparticles in the composites. Structural changes are observed at TiN ≥ 30 wt %, where the in situ synthesis results in rod-shape composite particles. The electrical and electrochemical properties of the nanocomposites were also affected by the structure. The mechanisms of the property changes with the TiN contents are discussed. The structural difference was used to explain the different activation energies for the conductance process in emeraldine base (EB)/TiN composites.

1. Introduction

Polyaniline (PANI) is known as one of the most promising conducting polymers due to the ease of preparation and good environmental stability combined with moderate electrical conductivity.[1−11] In recent years, the incorporation of inorganic components into PANI has led to unique composites exhibiting enhanced conductivity[12−14] and special mechanical,[15,16] electronic,[17] electrochemical,[18−20] and optical,[21] as well as magnetic, properties.[22,23] Such new hybrid polymer/inorganic composites have a large variety of applications including in electrochromic devices, light-emitting diodes, chromatography, secondary batteries, electrostatic discharge protection, and sensors for gases. For example, the PANI/carbon nanotube shows high electroactivity and is an excellent electrode material in plastic transistors.[24] PANI/V_2O_5 offers considerable promise for utilization as a cathode for lithium secondary batteries due to the relatively high conductivity and the increased specific capacity.[18,25] PANI/zeolite possesses antiferromagnetism compared with paramagnetic pure PANI,[22] while PANI/maghemite is superparamagnetic.[26] Many other PANI/inorganic nanocomposites with diverse structures have also been reported, such as silica,[16] TiO_2,[17,21] ZnO,[27] WO_3,[28] Sn,[29] etc., in the past few years. In this background, new PANI/inorganic nanocomposites are triggering more and more interests from both pure and applied scientists.

Although many papers on PANI/oxide and other PANI/inorganic composites have been published, few research projects dealing with PANI/nitride composite have been reported yet. One possible reason is that the applications of nitrides are limited to some certain areas at present, such as machinery and structural components (Si_3N_4, BN), protective coatings (TiN, CrN), and electronic applications (AlN, GaN).[30−32] In addition, nitrides are much more difficult to synthesize relative to their oxide counterparts. Special apparatus and/or high temperature are often needed for the synthesis, which makes the preparation of polymer/nitride composites inconvenient and infeasible. To obtain a hybrid PANI/nitride material, nanosized nitride particles should be synthesized first. Then they can be easily incorporated into the PANI matrix by in situ polymerization on nanoparticles or by a conventional sol−gel process. At the same time, the entrapping of nitride nanoparticles may bring new electrical, optical, and magnetic properties to PANI as some superior properties have been discovered on many nitrides. Furthermore, incorporating nitrides into conducting polymers can greatly enlarge the application extent and enhance the processibility of nitride materials. It is also very interesting from a scientific point of view to produce and study a hybrid polymer/nitride compound as a totally new material system, which has never been studied before.

Following these ideas, we present in this paper the first successful in situ preparation of a new class of PANI/nitride nanocomposite materials by in situ polymerization. Titanium nitride (TiN) is well-known for its oxidative stability, corrosion resistance, and good electrical conductivity, which makes TiN an excellent candidate for electrodes in electrochemical capacitors in highly corrosive electrolytes and in semiconductor devices.[33−36] The present study demonstrated that PANI/TiN has a relatively high conductivity and a good electroactivity. The structures and properties of the composites are controlled by the TiN content. The possibility of utilizing PANI/TiN nanocomposites as cathodes in Li batteries was also investigated.

2. Experimental Section

1. Reagents. All reagents were analytical grade and were used as received from Shanghai Chemical. Ammonia (>99% purity) was purchased from Lixin Gas Co. Distilled water was used in all experiments.

2. Preparation of TiN Nanoparticles. For the preparation of TiO_2 precursors, 11 mL of a 3 M $TiCl_4$ solution was mixed

* Address correspondence to this author. E-mail: liangaoc@online.sh.cn. Fax: +86-21-52413122. Phone: +86-21-52412718.

10.1021/jp053845b CCC: $30.25
Published on Web 09/24/2005

with 19 mL of a $(NH_4)_2SO_4$ solution and the $[Ti^{4+}]$:$[SO_4^{2-}]$ molar ratio reached 1:2. Then the mixed solution was heated to 70−90 °C and maintained at the same temperature for 1 h. Subsequently, 2.5 M dilute NH_4OH was added dropwise into the solution under high-speed stirring until the pH value reached 6−7. The precipitates were filtered and repeatedly washed with distilled water and ethanol, then vacuum-dried at 60 °C. After being calcined at 400 °C for 2 h, anatase TiO_2 nanoparticles were obtained with an average size <20 nm. TiN nanoparticles were made by our standard procedure.[36a] The nanocrystalline TiO_2 powder was loaded in a quartz boat and heated in flowing ammonia gas of 1 L min^{-1} at 800 °C for 5 h in a tube furnace. The heating rate was 10 °C min^{-1} before reaching 800 °C. After the nitridation was completed, the furnace was turned off and the TiN powder was cooled to room temperature naturally in the flowing NH_3 gas. The obtained TiN powder was characterized by XRD and TEM.

3. In Situ Polymerization of PANI on TiN Nanoparticles. In a typical procedure, the desired quantity of TiN nanoparticles (ranging from 0 to 0.9 g) was ultrasonically dispersed in 100 mL of 1.5 M hydrochloric acid containing 1.86 g of aniline. The solution was precooled in an ice bath and the $(NH_4)_2S_2O_8$ was added in the form of a 1 M solution (20 mL) to the reaction mixture, which was stirred for 60 min and left standing for 120 min without stirring. The resultant composite powder was filtrated and washed thoroughly with water and ethanol, and then dried under vacuum at 60 °C for at least 12 h, resulting in the partially doped PANI composites.

In a control experiment, TiN nanoparticles were treated exactly in the same way without adding aniline to investigate the effect of experimental procedures on the electrical conductivity of TiN. TiN nanoparticles were ultrasonically dispersed in $HCl/(NH_4)_2S_2O_8$ solution and stirred for 60 min and left standing for 120 min without stirring. The powder was filtrated and washed thoroughly with water and ethanol, and then dried under vacuum at 60 °C for at least 12 h, resulting in the acid-treated TiN nanopaticles.

Some of the in situ prepared PANI/TiN composite solids were stirred with 3 wt % ammonium hydroxide for 48 h. Then the emeraldine base (EB) composite was isolated by filtration and washed with water and ethanol until pH 7. The EB/TiN was dried under vacuum at 60 °C for at least 12 h.

To make a comparison with PANI/TiN nanocomposites, pure PANI and TiN nanoparticles were mixed manually by grinding in a mortar and the conductivities and electrochemical properties of the physical mixtures (denoted as PANI+TiN) were also measured.

4. Structural Characterization and Measurements of Electrical and Electrochemical Properties. The surface composition and chemical structure of the acid-treated TiN nanoparticles was analyzed by X-ray photoelectron spectroscopy (XPS: MicroLab MKII, VG Scientific, Sussex, UK). FTIR analyses were performed in a Nicolet NEXUS spectrometer. The solid-state absorption spectra of PANI and composite powders were recorded directly with a Shimaszu UV-3101PC UV−vis spectrometer. X-ray powder diffraction was obtained in a Rigaku D/MAX 2550 V powder diffractometer, using Cu Kα radiation ($\lambda = 1.5406$ Å). The morphology was measured by a scanning electron microscope (JSM-6700F, JEOL) and a transmission electron microscope (200CX, JEOL) equipped with an energy-dispersive X-ray spectrometer (EDS). The samples were gold-sputtered prior to SEM observation. The sample for TEM observation was prepared by the following procedure: The composite powder was dispersed in ethanol through ultrasonic irradiation, and then the dispersion was dropped on a copper grid to observe the morphology of composite particle.

To measure the conductivity, the PANI/TiN composite powders were pressed into 6-mm pellets at 6 MPa. Then the conductivity at room temperature was measured by a standard four-probe van der Pauw method with an Accent HL5500 Hall System (U.K.). For less conducting EB/TiN composites ($\sigma < 10^{-7}$ S cm^{-1}), samples of the materials were pressed into 14-mm pellets (0.8-mm thick) at 20 MPa. Two copper leads were attached onto both sides of the pellets with silver paint. The conductivity between −70 and 150 °C was measured with a Keithley 6517A Electrometer/High Resistance Meter, using the force voltage measure current (FVMI) technique. The PANI/TiN composites were also pressed into pellets (150-mg mass, 14-mm diameter, and 0.8-mm thick) at 20 MPa to measure the impedance spectra at the Agilent 4294A Precision Impedance Analyzer (40 Hz−110 MHz) at room temperature.

Electrochemical measurements of PANI/TiN nanocomposite samples were performed with a three-electrode electrochemical cell, using an EcoChemie pgstat 30 potentiostat. The electrodes were made by pressing the sample powder (30 mg) onto a 14-mm nickel foam disk or by pressing 150 mg of each sample directly into a pellet (14-mm diameter and 0.8-mm thick) at 20 MPa. The silver paint was used as a contact to the copper wire. In 1 M aqueous HCl, the three-electrode system consisted of a PANI/TiN/Ni or PANI/TiN pellet as the working electrode, a Pt foil as the counter electrode, and a saturated calomel reference electrode (SCE).

5. Fabrication of a Li Battery. The used chemicals were purchased from Shanghai Chemical. All cells were assembled inside an Ar-filled glovebox (NAC-AM-2). Li foil was used as the negative electrode and a solution of 1 M $LiPF_6$ in a 1:1 mixture of ethylene carbonate and diethyl carbonate was used as the electrolyte. A microporous polypropy film (Celfard) was used as a separator. The cathode was a film made by ball-mixing the PANI/TiN composites (4 to 65 mg) and acetylene black and polyvinylidene fluoride (in 8:1:1 by weight) in *N*-methyl-2-pyrrolidinone for 24 h and subsequent spread on an aluminum foil. The solvent was evaporated at room temperature and a 14-mm disk was cut from the film. After further vacuum drying at 100 °C for 10 h, the pellets were assembled into the Li battery. Charge/discharge characteristics of the cells were recorded by a LAND CT2001A battery tester, using a constant current density of 125 mA g^{-1} (1.2 mA cm^{-2}) between 2.9 and 3.9 V at room temperature.

3. Results and Discussion

1. Characterization of PANI/TiN and EB/TiN. As synthesized TiN nanoparticles have been analyzed by powder X-ray diffraction and are shown in Figure 1. From the line broadening of corresponding XRD peaks, the mean size of TiN nanoparticles was estimated as about 19 nm according to the Scherrer equation. Such a small particle size makes it more easy to take place for the hydrolysis of TiN. In the control experiment, nanocrystalline TiN has 2θ values of 37.10°, 43.08°, 62.54°, 75.02°, and 79.04° after treated in HCl solution, slightly higher than the values of untreated TiN (37.02°, 42.98°, 62.36°, 74.70°, and 78.92°, the difference of 111 and 200 peaks is magnified in the inset of Figure 1). The lattice constant a_0 decreased from 4.205 to 4.196 Å after the treatment in acid solution, suggesting more oxygen was dissolved into TiN because of particle surface hydrolysis in acid solution.[36b,37] The XPS technique was used to determine the degree of surface hydrolysis of TiN nanoparticles. The results showed that the major elements of the acid-

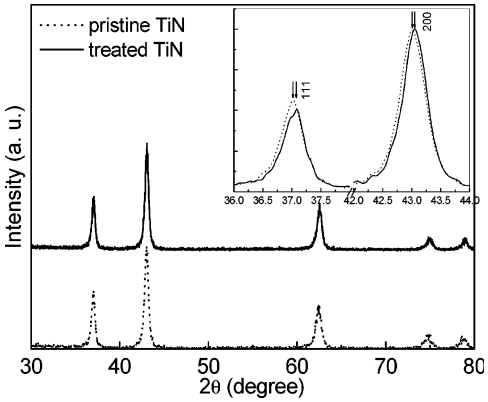

Figure 1. Powder XRD patterns of TiN nanoparticles. The difference between pristine and acid-treated TiN is enlarged in the inset.

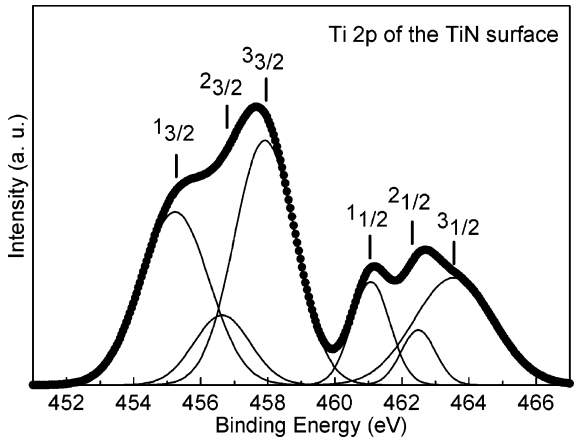

Figure 2. XPS Ti 2p spectra from acid-treated TiN nanoparticles. Note: subscript 3/2 and 1/2 mean Ti $2p_{3/2}$ and $2p_{1/2}$ spectra, respectively.

treated TiN particle surface were oxygen (42.1 atom %), nitrogen (37.3 atom %), and titanium (20.6 atom %). The abnormally high content of surface oxygen again provides evidence of formation of the hydrolyzed layers on the TiN nanoparticles. The peak fitted XPS core level spectra in the Ti 2p region for the hydrolyzed TiN nanoparticles was shown in Figure 2. Peak 1 corresponds to Ti−N. Peak 2 and peak 3 at higher binding energies are attributed to Ti−O−N and Ti−O_2, respectively.[35] The area ratio of peak 1:peak 2:peak 3 is about 1:0.4:1.6, which means surface Ti atoms were predominantly bonded to O atoms after hydrolysis. In addition, the control experiment showed clearly that no oxide phase was formed after the treatment in HCl/$(NH_4)_2S_2O_8$ solution.

UV−vis absorption spectra of PANI and PANI/TiN powders with different contents of TiN are shown in Figure 3a. As one can see, the characteristic peaks of PANI appear at 314 and 629 nm, which are attributed to $\pi-\pi^*$ transition in the benzenoid rings and the localized exciton peak associated with the quinoid ring, respectively.[10] Small absorption shoulders near 380 and 780 nm associated with polaron-π^* and π-polaron transitions, respectively, can also be observed in the spectra, along with a free carrier tail extending into the near-infrared region (>800 nm).[10,38] The results suggest that the prepared PANI is in partially doped form.[7] For PANI/TiN composites with a TiN content of 15 and 30 wt % (denoted as PANI-15 and PANI-30), they show almost the same absorption peak with PANI. Furthermore, the peak shape of PANI/TiN composites is in good accord with those of PANI. The characteristic absorption of TiN nanoparticles at 555 nm is completely eliminated from the spectra of the composites. In contrast, the PANI+TiN mixture (containing 50 wt % TiN) shows the absorption of the simple sum of the individual contributions from PANI and TiN powders (line 5, Figure 3a). Thus, it is reasonable to deduce that TiN nanoparticles are almost completely coated by PANI (i.e., incorporated inside PANI particles) by in situ polymerization, and do not form a separated phase from PANI particles. It should be mentioned that the quantities of the powders are the same in all the absorption measurements. Thus it is interesting to note that the absorptions of both benzenoid rings and quinoid rings are abnormally strengthened with the increased content of TiN (lines 1 to 3, Figure 3a), which should be due to the interaction between TiN nanoparticles and PANI coatings.[18] The intensity of the polaron bands at ~380 and ~780 nm also increases with the increasing amount of incorporated TiN nanoparticles, which would suggest a higher conductivity. The dependence between the TiN content and the conductivity will be investigated in the following section.

To further understand the interaction between TiN nanoparticles and PANI, we used FTIR spectroscopy to characterize the molecular structure of PANI and PANI/TiN nanocomposites. The major characteristic peaks are summarized in Table 1. The IR spectrum of PANI (Figure 4a) shows characteristic bands at 1564 (assigned as C═C stretching of the quinoid rings), 1480 (C═C stretching of benzenoid rings), 1300 and 1239 (C−N stretching of secondary aromatic amine), and 1118 cm^{-1} (N═quinoid═N). The 1564 and 1484 cm^{-1} modes show a red-shift compared to those of EB (Figure 4c), which indicates the PANI is partially doped.[8] The typical IR spectrum of PANI/TiN (Figure 4b) has an overall similarity with that of PANI, but it is noted that the N−H stretching mode is red-shifted from 3446

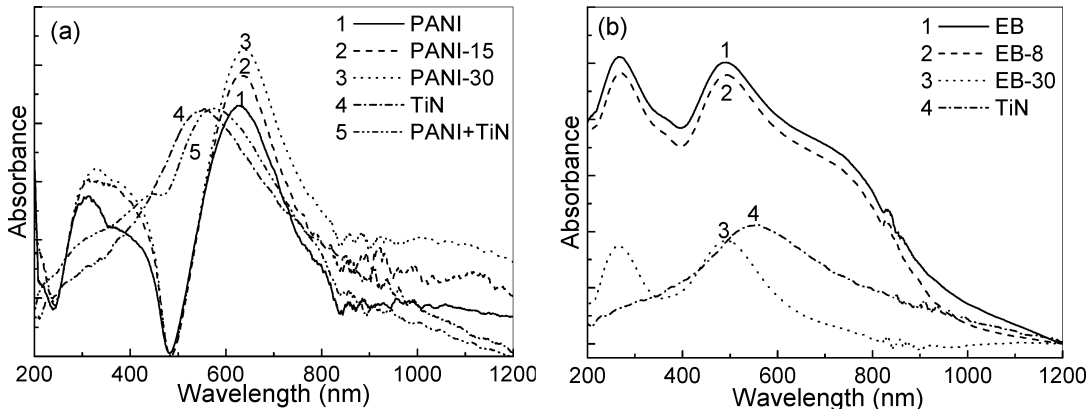

Figure 3. UV−vis absorption spectra of (a) PANI/TiN composites and (b) EB/TiN composites with different TiN contents and their constituents. The minor peaks at 800−1000 nm arise from the spectrometer.

TABLE 1: Characteristic Peaks (cm^{-1}) of the IR Spectra of PANI, PANI/TiN, EB, and EB/TiN[a]

assignment[b]	PANI	PANI/TiN	EB	EB/TiN[c]
str of free N−H	3446	3430 ↓	3320	3420 ↓
str of C═C (Q)	1564	1564	1593	1588 ↓
str of C═C (B)	1480	1480	1502	1497
str of C−N	1300, 1239	1300, 1239	1308, 1238	1300, 1232
a mode of N═Q═N	1120	1120	1168	1160
ben of Caromatic-H	801	801	831	826

[a] From refs 5, 8, and 11. [b] str = stretching; ben = bending; Q = quinoid unit; B = benzenoid unit. [c] The ↓ means a decreasing in intensity relative to that of pure polymers.

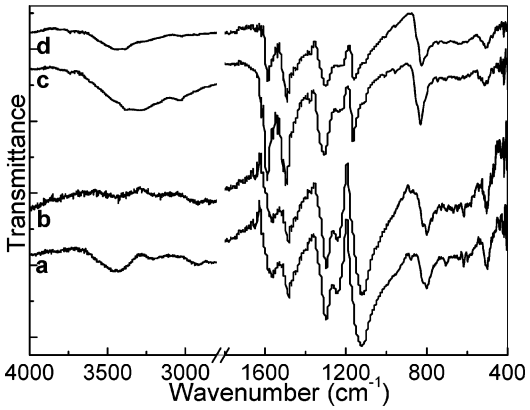

Figure 4. FTIR spectra of PANI (a), PANI/TiN (b), EB (c), and EB/TiN (d). The spectra are offset for clarity.

to 3430 cm^{-1}. At the same time, the intensity of free N−H stretching mode dramatically decreased in the composite. Xia et al. found the incorporation of nano TiO_2 led to the decrease of N−H peak intensity.[38] Zengin et al. prepared EB-CNT composite and found CNT perturb the H-bonding and increase the N−H stretch intensity.[13] Niu et al. found that the H-bonding between PANI and silica gel caused the red-shift of the NH stretching mode (from 3452 to 3444 cm^{-1}).[39] Thus, the origin of the change of the N−H peak is suggested, according to the FTIR results and previous studies,[38,39] resulting from the formation of hydrogen bonds between polyaniline and the functional groups (e.g. −OH) on the surface of hydrolyzed TiN nanoparticles.

After being washed with 3 wt % NH_4OH, the $\pi-\pi^*$ transition and the exciton band exhibited a dramatic blue-shift from 314 to 267 nm and from 629 to 495 nm, respectively (Figure 3b). The shift of absorption after dedoping to the EB form was similar to that reported earlier.[2] Corresponding, the color of the EB powder changed from dark green to dark purple. The absorptions decrease with the decrease of EB content (lines 1 to 3, Figure 3b), which is different from the spectra of PANI/TiN composites. The reason for this difference is not clear at present, but is thought to be related to the state change of the −NH group in EB form.[13] The FT-IR spectra of EB powder and EB/TiN composite (Figure 4c,d) also find new changes. Their major characteristic peaks are summarized in Table 1. The vibration peaks accord well with the literature values.[5,8] By dedoping the PANI with ammonium hydroxide, the intensity of the quinoid peak at 1593 cm^{-1} increased at the expense of a decrease of benzenoid rings at 1502 cm^{-1}. At the same time, the band at 1168 cm^{-1} relating to the conductivity was weakened relative to that of PANI.[13] For the EB/TiN composite, the major characteristic peaks shifted by 5−8 cm^{-1} relative to those of EB. The intensity of the quinoid peak at 1588 cm^{-1} undergoes a decrease. In addition, the N−H stretching peak, which shifted to the higher frequency of ∼3420 cm^{-1}, becomes much weaker as in the case of the PANI/TiN composite.

Summarizing the results of XRD, UV−vis, and FT-IR analysis, we believe that in situ polymerization of aniline on the base of TiN nanoparticles forms composite materials. The interaction between the outer PANI (or EB) layer and the inner TiN nanoparticles is confirmed. The hydrolysis of TiN nanoparticles in acid solution could generate abundant hydroxyl groups (−OH) on the large surfaces of nanoparticles,[40] which formed hydrogen bonds with the amino/imino group of PANI. The incorporated TiN nanoparticles interact with doped PANI through hydrogen bonding, which caused the strengthened UV−vis absorption and the changes of IR vibration. After being washed with NH_4OH solution, the state of the polymer changed, but the interaction still existed. In both cases, the TiN nanoparticles are incorporated in polymer particles, forming a real composite phase instead of a separate phase. The determinative and direct proofs come from TEM observations (see the next section).

2. Microstructures. Parts a and b of Figure 5 show the typical SEM micrographs of polyaniline/TiN composite and pure PANI, respectively, indicating a slight increase in particle size (approximately from 50 nm to >100 nm). That is, the incorporation of TiN nanoparticles will influence the morphology of the resulting PANI/TiN.[11,17,23] The magnification of the images is too low and more detailed microstructures should be observed with TEM.

To make a comparison, TEM photographs of pure PANI and the PANI+TiN physical mixture are first shown in Figure 6, parts a and b, respectively. After being nitrided in ammonia at 800 °C, formation of spherical TiN particles with average particle diameter about 20 nm was observed (see Figure 6b), which is consistent with the XRD estimation.[36a] In the absence of nanocrystalline TiN, the long particles of polyaniline prepared

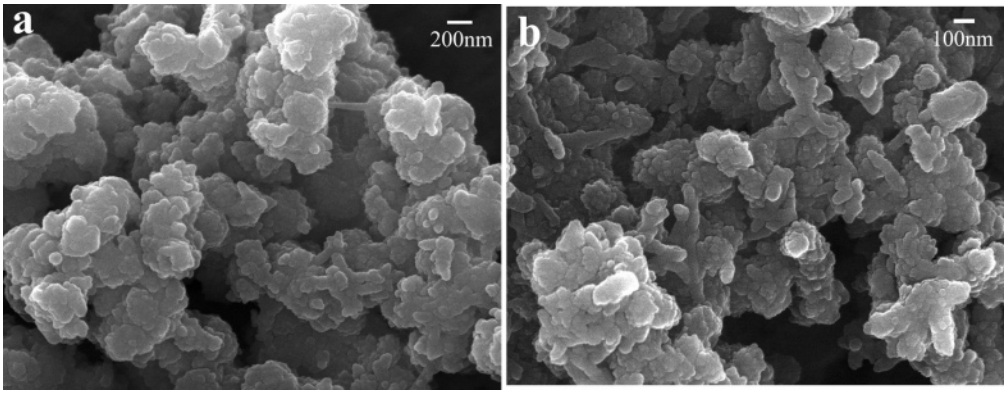

Figure 5. SEM images of (a) PANI/TiN composite and (b) pure PANI.

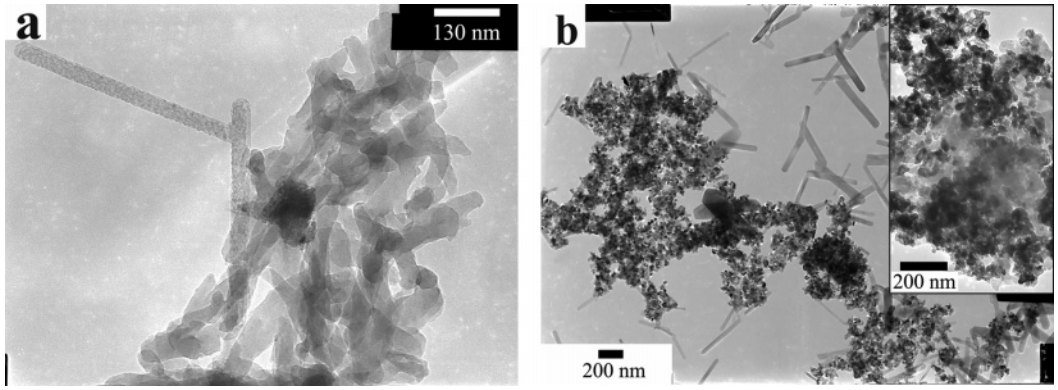

Figure 6. TEM photographs of (a) pure PANI and (b) physical mixture of PANI and TiN nanoparticles.

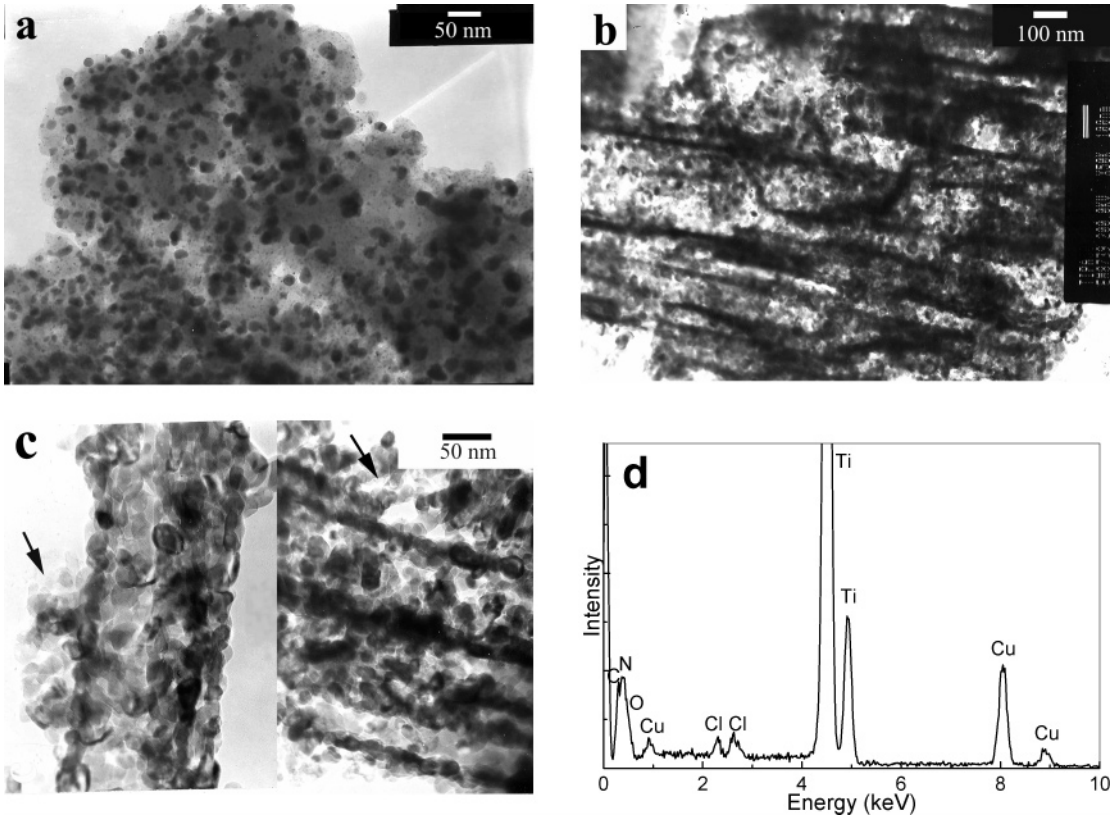

Figure 7. TEM photographs of PANI/TiN composite: (a) PANI-15, 15 wt % of TiN charged, and (b) PANI-50. (c) The detailed structure of individual PANI-30 composite rod (left) and agglomerated PANI-50 (right) composite rods under higher magnification. (d) EDS data obtained from PANI-50 composite rods.

by chemical oxidation are 30−150 nm in length and 20−50 nm in width with an irregular shape, as shown in Figure 6a. Some particles grew into longer rods and the length can reach ~500 nm. After grinding PANI and TiN together in a mortar, it can be seen from Figure 6b that they are still two distinct phases. Some TiN particles may be pressed into an amorphous PANI matrix by force (shown in the inset of Figure 6b), but they do not form real composite material.

Through the in situ chemical oxidative method, real PANI/TiN nanocomposites were obtained. The TEM photographs of polyaniline/TiN composite particles are shown in Figure 7. It can be clearly seen from Figure 7a−c that black TiN nanoparticles are completely incorporated and dispersed homogeneously within the amorphous PANI matrix in PANI-15 composite. It was found that the morphology and structure of the resulting PANI/TiN composite could be controlled by the content of TiN nanoparticles. When the TiN content was low, TiN nanoparticles were embedded in a featureless amorphous polymer matrix (Figure 7a). When the load of TiN nanoparticles was as high as 30 wt %, TEM observes that the PANI particles began to grow into an individual rodlike structure with a diameter of 100−300 nm and a length up to a micrometer (Figure 7c, left). At a higher TiN content of 50 wt %, most of the TiN nanoparticles have been incorporated into composite rods. At the same time, these composite rods tend to agglomerate side-by-side with each other, as shown in Figures 7b and 6c, right. The TiN nanoparticles were embedded in the composite rods and, at the same time, aligned spontaneously along the edges of the rods. More structural details can be seen from Figure 7c, which shows the rods are embedded with TiN particles, with edges made up of a row of TiN nanoparticles sticking one by another by PANI. Similar self-assembled rod (or tube) structures were observed in other PANI/nanoparticles composites such as PANI/TiO_2[12] and PANI−NSA/Fe_3O_4.[23] The composition of the composite rod was further confirmed by synchronous EDS measurements, which revealed that the titanium element is

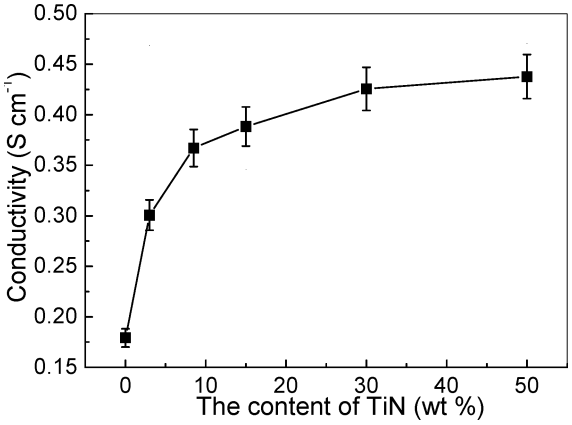

Figure 8. Variation of conductivity of PANI/TiN composites at ambient temperature with the content of TiN.

clearly seen to be in the composite rods as shown in Figure 7d. The oxygen signal should arise from the hydrolyzed TiN surface as suggested by XPS, although the contribution of adhered O could not be ruled out completely.

Especially, it was noted that some uncoated TiN nanoparticles were observed outside the composite rods as pointed out by arrows in Figure 7c. It should be mentioned that the UV−vis spectrum of PANI-30 and PANI-50 did not show any characteristics of TiN absorption, indicating the amount of uncoated TiN particles is small. However, a small quantity of uncoated nanocrystalline TiN can greatly affect the electrochemical property of the resulting composites (detailed discussion is seen in section 3.4).

By comparing the morphology of in situ prepared PANI/TiN composites (Figure 7a−c) and physically mixed PANI+TiN (Figure 6b), it is found that, different from PANI/TiN materials obtained through in situ polymerization, PANI+TiN is a simple mixture of PANI particles and TiN aggregates. The TiN particles are separated from the PANI matrix and aggregate heavily. This is because the aggregates of nanocrystalline TiN are difficult to break down by grinding. Ultrasound can help to break the aggregates of nanocrystalline TiN[38] and during this approach the aniline molecules can adsorb onto the particle surface through hydrogen bonds. After adding $(NH_4)_2S_2O_8$, the adsorbed polyaniline can form a polymerized layer on TiN particle surfaces, which is advantageous to achieve a homogeneous dispersion of TiN nanoparticles in the PANI matrix. Thus through the in situ polymerization and particle growth, real PANI/TiN composite materials can be obtained.

3. Electrical Properties. The variation of room-temperature conductivities of PANI/TiN nanocomposites with TiN weight fraction is as depicted in Figure 8. The conductivity of the nanocomposites increases continuously with the increasing TiN content. When the content of TiN reaches 8%, the conductivity of composite is doubled. Further increase of TiN content improves the conductivity only marginally. Nevertheless, the conductivities of PANI/TiN composites are still at the same order as that of polyaniline. A possibility is that the TiN nanoparticles are coated with the PANI layer, thus hindering the direct contact between TiN nanoparticles to form conductive networks. Another reason is that the surface of TiN particles was hydrolyzed in the acid solution during the in situ polymerization of PANI, generating a nonconductive hydrolyzed layer. As a control experiment, the TiN nanoparticles alone were added in 1.5 M hydrochloric acid and treated by the same method. We measured the electrical conductivity of the pristine TiN and acid-treated TiN by the four-probe technique after compression

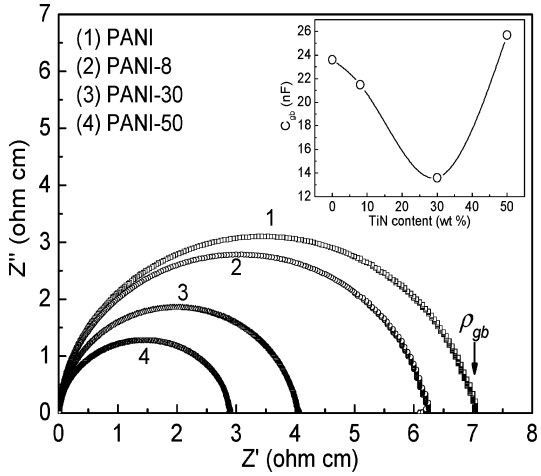

Figure 9. Room temperature ac impedance data for different PANI/TiN nanocomposites.

of the powder into pellets. The conductivity of TiN decreases by an order of magnitude from about 500 to 75 S cm^{-1} after the acid treatment, which gives unambiguous evidence of the formation of a hydrolyzed layer on the surface of TiN nanoparticles.

To investigate the effect of the in situ polymerization method on composite conductivity, the conductivities of the physical mixtures of PANI and TiN were measured. The conductivities of PANI+TiN mixtures (containing 8−50 wt % TiN) varied irregularly in the range between ∼0.2 and 0.5 S cm^{-1} and the value did not suggest any apparent correlation with the TiN content. It is because the direct mixing of two components cannot achieve a homogeneous composite material.

Room-temperature ac impedance measurements were carried out to study the contribution of the grain boundary resistance. The PANI/TiN composite pellets were pressed at 20 MPa without sintering due to the limited thermal stability of PANI. A single semicircle is seen in the complex impedance plane (Figure 9), which means the grain boundary resistance dominates the overall impedance.[41] The value of their grain boundary capacitance, C_{gb} = 10−30 nF, found from the maximum of each semicircle, using the relation $\omega_{max}RC = 1$, is consistent with this assignment.[19,41] Thus it is concluded that the total resistance of the nanocomposites is determined predominantly by the grain boundary factor. It is also found that the boundary resistivity (ρ_{gb}) decreases from 7.0 to 2.9 Ω cm (the conductivity increases from 0.14 to 0.35 S cm^{-1}) with the increasing TiN content, which is consistent with the results measured by the four-probe technique. In the composites, the PANI particles grow into integrated homogeneous composite particles in the presence of TiN nanoparticles, which causes the decrease of grain boundary area as well as the resistivity. Since the impedance spectrum is sensitive to the material structure, it can be used to uncover the structure change of PANI/TiN. As shown in the inset of Figure 9, the C_{gb}-TiN content relationship exhibits a turning point at TiN content = 30 wt %, which clearly indicates the grain boundary structure, i.e., the composite structure, begins to change at this point. This result coincides well with the TEM results that the rod-shape composite particles begin to from at TiN content = 30 wt % as discussed in section 3.2.

After being dedoped with NH_4OH solution, the conductivity of EB/TiN composites dropped dramatically by more than 9 orders of magnitude to 10^{-10}−10^{-11} S cm^{-1} at room temperature. The temperature dependence of dc conductivities for both EB and EB/TiN composites exhibits a typical semiconductor

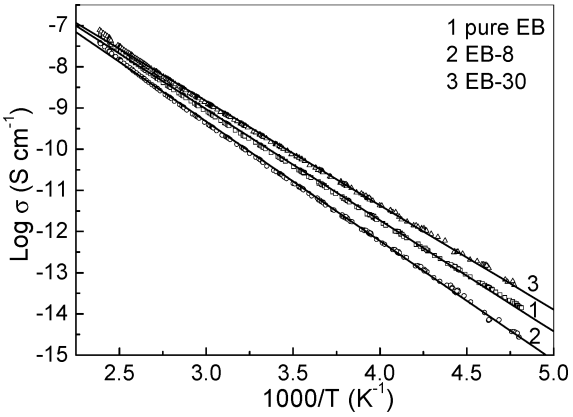

Figure 10. Arrhenius plot of the conductivities of EB and EB/TiN composites versus 1000/*T*.

behavior: the conductivity of all samples measured in the range 205−420 K decreased with decreasing temperature as shown in Figure 10. In addition, all sets of data are in very good agreement with Arrhenius law (eq 1) over the range of temperatures studied.

$$\sigma = \sigma_0 \exp(-E_a/kT) \tag{1}$$

From the slope of the linear fit the activation energy (E_a) for the conductance process is calculated, obtaining a value of 22.4 (0.23 eV), 24.3 (0.25 eV), and 21.0 kJ mol^{-1} (0.22 eV) for pure EB, EB-8, and EB-30, respectively. All E_a values are higher than the ones reported for conducting polymers.[19,42] No thermal transitions over this temperature range are evident, suggesting that these materials are thermodynamically stable in this range. The change in the activation energy gave unambiguous evidence supporting the interaction of PANI with TiN. It should be noted that E_a of EB-8 is higher while E_a of EB-30 is lower than that of pure EB. This difference reveals that the two composites are in distinct morphologies (e.g. structures) as discussed above. When the TiN content was higher than 30%, the composite rods began to form. The TiN nanoparticles are adhered closely with each other in the composite rods and the rods have a large aspect ratio, which favor the conductance of electrons. Meanwhile, the uncoated TiN nanoparticles may promote the intertransportation of electrons between adjacent composite rods. Thus the activation energy of EB-30 is lower than both EB and EB-8. It should be noted that the effect of composite structure on the electrical conductivity is evident only in less conductive EB/TiN composites. For highly conductive PANI/TiN composites, the effect of the structure is less important as discussed above.

4. Electrochemical Properties. It is well-known that the performance of a resistive electrode can be improved by adding a conducting agent into it. Although the conductivity of PANI/TiN does not change much with the TiN content, the electrochemical behavior is greatly affected by the incorporated conductive TiN. We investigated the influence of in situ incorporated TiN nanoparticles on the electrochemical properties of the less conductive PANI electrode. Figure 11a shows the cyclic voltammograms (CV) of TiN, PANI, and PANI/TiN composites versus a standard calomel reference electrode in a 1.0 M HCl aqueous solution. All the CV data obtained from the PANI/TiN/Ni electrodes have a featureless and narrow-string shape, thus the electrochemical properties discussed below are based on the data obtained directly from PANI/TiN pellets. The recorded CV of the pure PANI electrode resembled that of PANI dense films prepared by Wang et al.[10] The total shapes of CV curves of PANI/TiN electrodes are analogous to that of PANI. They both show only one broad reduction peak, corresponding to the changes in oxidation states from emeraldine to leucoemeraldine.[1,10] With the increase of TiN content, the reduction peak of PANI/TiN becomes more anodic than that of polyaniline, and this behavior suggests the formation of a conducting composite of polyaniline and TiN. In addition, for 8% and 15% TiN incorporation, both the curves were shifted to more negative values and a higher reduction peak current was recorded. If there were no molecular-level interaction between PANI and TiN, the signals for the PANI/TiN composites in Figure 11a should be the arithmetic sums of the signals of PANI and TiN. However, the greater redox peak currents than the arithmetic sum of the individual contributions show clearly that interaction occurs. Thus we believe that incorporating TiN nanoparticles into PANI can lead to a material with a stronger electrochemical activity, possibly due to the hydrogen bonding between the components, which facilitates electrochemical reactions.[18]

For further understanding the enhancing effect of TiN nanoparticles on the electroactivity of PANI, we calculated the specific capacitance of the electrode materials. The specific capacitance (C) of an electrode may be defined by the relation

$$C = \frac{1}{\upsilon(V_a - V_c)} \int_{V_a}^{V_c} J(V)\, dV \tag{2}$$

where υ is the scan rate, $V_a - V_c$ is the potential range, and I is the current. For composite electrode materials, m is the total mass of the electrode material (PANI and TiN). The specific capacitance of polyaniline obtained from the TiN-incorporated electrode was larger, as much as 76.4 and 79.8 F g^{-1} for PANI-8 and PANI-15, respectively, than both 52.8 F g^{-1} for the pure PANI electrode and 31.6 F g^{-1} for the pure TiN electrode (Figure 11d). That is, by in situ adding 8 and 15 wt % TiN into PANI, the specific capacitance is increased by 45% and 51%, respectively, relative to that of the pure PANI electrode. From this result, it is known that incorporation of conducting TiN into the PANI electrode increases the specific capacitance of the electrode material. Although TiN particles did not make a continuous electron path, the incorporated conducting TiN generates more active sites for the faradaic reaction (transfer of charge through the interface) inside the electrode by making good contacts with the PANI matrix, thus PANI particles located far from the electrode surface can take part in the faradaic reaction for pseudocapacitance.[43] Otherwise, the faradaic reaction could arise only in the restricted region near the electrode surface because of the low conductivity of as prepared PANI. In addition, the double layer effect on the interface between TiN nanoparticles and the PANI matrix must make a contribution to the capacitance. Hence, we believe that the TiN-incorporated electrode exhibiting higher specific capacitance is due to more available active site area around the incorporated TiN nanoparticles as well as the double layer effect. Indeed, the measured specific capacitances should be less than the real values considering the thickness of the PANI/TiN pellets. We are currently measuring less charge than could be stored in the interior.

However, the larger amounts of TiN (30−50%) did not bring about further improvement in electrode performance. The specific capacitance decreased with further increasing of TiN contents, from 79.8 to 61.0 (30% TiN) and to 31.6 F g^{-1} (50% TiN), which is almost the same with that of the pure TiN electrode (Figure 11d). This can be related to a different microstructure of the composites. As is discussed above, when TiN content is high (≥30 wt %), PANI cannot cover all of TiN nanoparticles during the polymerization, leaving some uncoated

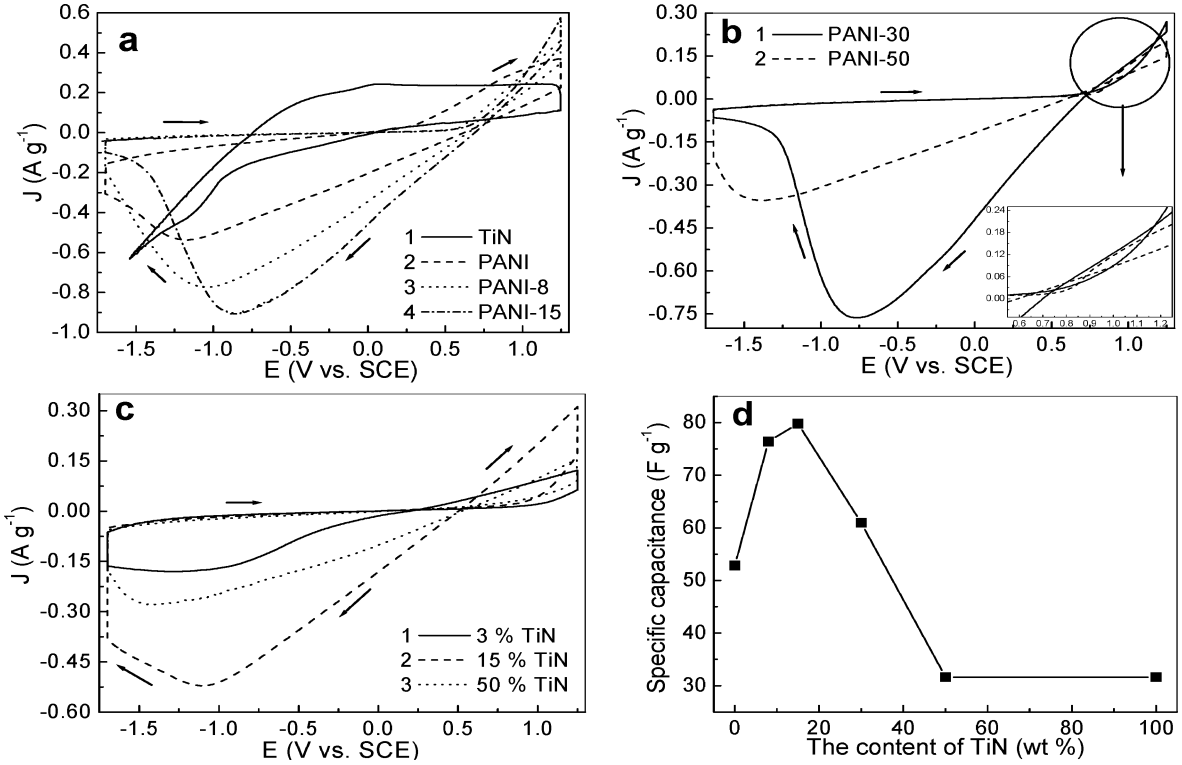

Figure 11. Cyclic voltammograms performed at a scan rate of 5 mV s^{-1} between −1.7 and 1.25 V (vs SCE) in a 1.0 M HCl aqueous solution at room temperature: (a, b) pure PANI and PANI/TiN composites and (c) physical mixtures of PANI and TiN. The current has been normalized with respect to the mass of the electrode materials. The variation of calculated specific capacitance with the content of TiN is shown in part d.

particles outside of the composite rods (pointed out by arrows in Figure 7c). Another important difference is the so-called "nucleation loop" or crossing-over of the cathodic and anodic branches, which is shown in the inset of Figure 11b. It is noted that the pure TiN electrode does not show this nucleation phenomenon (Figure 11a). By correlating the decrease in the specific capacitance and the nucleation process of the TiN component, we speculate that high TiN content will result in the nucleation process of uncoated TiN nanoparticles exposed outside the composite particles, and thus lead to the decrease in the specific capacitance. Optimal performance was found for 15% addition of TiN, which gives a complete PANI-coated composite structure.

CV curves recorded at the electrode prepared from physically mixed PANI+TiN powders are presented in Figure 11c. The three curves represent the typical nucleation loop similar to those of PANI/TiN electrodes with TiN ≥ 30 wt %, even at an adding amount as low as 3%. From the TEM observation (Figure 6c), it is known that the microstructure is quite different from in situ-prepared composite. All the TiN nanoparticles in the PANI+TiN mixture locate outside PANI particles, viz. contact directly with aqueous HCl electrolyte instead of isolated by PANI coating. This result is consistent with the assumption that nucleation process can take place at the noncoated TiN particles in PANI/TiN composites even when their amount is small. However, at this stage, it is difficult to evaluate how the nucleation occurs and affects the capacity character. At the same time, we believe that more studies are needed to investigate the exact mechanism of enhancement in electrochemical properties in more detail.

5. Battery Analyses. To be used as cathodes in lithium rechargeable batteries, 14.6 mg of PANI-50 composite powder was mixed with polyvinylidene fluoride (10 wt %) and acetylene black (10 wt %) to obtain films on aluminum foil. This cathode was tested in lithium batteries at a constant current density of

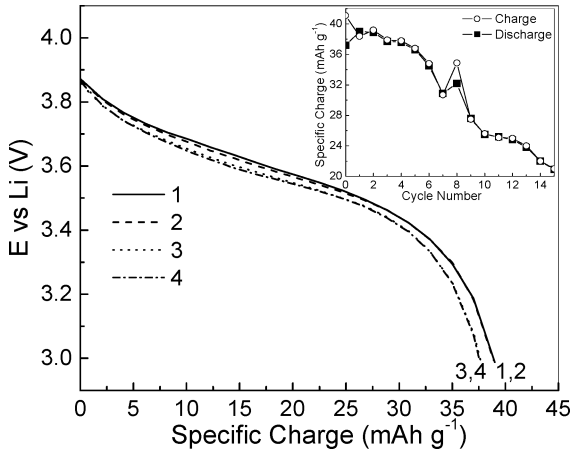

Figure 12. Discharge curves of PANI-50 film in the first 4 cycles: j = 125 mA g^{-1}. The inset shows the evolution of specific charge and discharge capacities upon cycling.

125 mA g^{-1} (1.2 mA cm^{-2}). The first four discharge curves operating between 3.9 and 2.9 V are shown in Figure 12. The discharge capacity at the first cycle was 38.9 mAh g^{-1}, which is close to the reported value, but the current density is much higher in this study.[19,44] The variation of specific capacity against cycle number for PANI-50 electrodes is shown in the inset of Figure 12, which illustrates the charge−discharge capacity decayed from 38.9 to 20.9 mAh g^{-1} over 15 cycles. This decay takes place because the composite films scale off from aluminum foil upon cycling. More severe problems were encountered when the TiN content was low, for example, for pure PANI or PANI-15. It is very difficult to make them into films or press them onto a Ni gauze because they will chap and peel off easily after drying. Thus the long-term cycling performance is largely determined by the PANI matrix binding strength. In addition, the physical mixtures of PANI and TiN showed a poor and

nonreversible charge−discharge performance. More efforts are currently underway to find more feasible methods for utilizing PANI/nitride nanocomposites in rechargeable Li batteries.

4. Conclusions

In conclusion, a novel composite of polyaniline containing TiN nanoparticles was successfully produced through the in situ polymerization method for the first time. The complete incorporation of TiN nanoparticles into PANI particles and a homogeneous dispersion of TiN phase were achieved. The results of XRD, FTIR, and UV−vis showed that the interaction between polyaniline and nanocrystalline TiN is strong. Hydrogen bonding between the functional group of hydrolyzed TiN nanoparticles and the outer PANI coatings was proposed to interpret the interaction between TiN and the PANI matrix. It was found that the morphology and structure of in situ-prepared PANI/TiN nanoparticles are controlled by the content of TiN. At the same time, their electrical properties and electrochemical properties of the PANI(EB)/TiN nanocomposites were also affected by the content of TiN. Impedance spectra, temperature dependence of conductivities, and CV analyses show that the structure change of the nanocomposites begins at a TiN content of ∼30 wt %.

The electrical resistance of PANI/TiN arises mainly from the grain boundary. When TiN content was low, both the conductivity and specific capacitance were enhanced with increasing TiN content, due to the increase of active sites for faradaic reaction and the double layer effect. The highest specific capacitance result was obtained with the PANI/TiN composite containing 15 wt % TiN, exhibiting an increase of 51% in the specific capacitance. The TiN nanoparticles were completely incorporated in polyaniline particles with good dispersion. When TiN content was 30 wt % or higher, the aggravation of the capacitance was observed, which was proposed to be related to the nucleation process of uncoated TiN nanoparticles. The impedance spectra of PANI/TiN composites show that C_{gb} changes with the composite structure. In addition, the temperature-dependent conductivities of EB/TiN composites also revealed that different composite structures had different E_a for electrical conduction. Lower E_a values were obtained at the composite with higher TiN content. In addition, the PANI/TiN nanocomposites may work as the cathode in the Li battery on the basis of further study. The specific capacity of PANI-50 can approach 40 mAh g^{-1} under a current density of 125 mA g^{-1} in the present study. This work thus demonstrates a feasible method to control the structure and properties of polyaniline/nitride composites and the potential of novel PANI/nitride nanocomposites for conducting components, capacitors, and lithium secondary batteries.

Acknowledgment. Special thanks are given to Dr. Xiangfeng Zhang for measuring charge−discharge curves and impedance spectrum. The authors also thank Prof. X. F. Hu for CV measurements.

References and Notes

(1) Lu, W.; Smela, E.; Adams, P.; Zuccarello, G.; Mattes, B. R. *Chem. Mater.* **2004**, *16*, 1615.
(2) Yuan, G. L.; Kuramoto, N. *Macromolecules* **2002**, *35*, 9773.
(3) Porget, J. P.; Józefowicz, M. E.; Epstein, A. J.; Tang, X.; MacDiarmid, A. G. *Macromolecules* **1991**, *24*, 779.
(4) Deore, B. A.; Yu, I.; Freund, M. S. *J. Am. Chem. Soc.* **2004**, *126*, 52.
(5) Quillard, S.; Louarn, G.; Lefrant, S.; Macdiarmid, A. G. *Phys. Rev. B* **1994**, *50*, 12496.
(6) Wei, Z.; Zhang, Z.; Wan, M. *Langmuir* **2002**, *18*, 917.
(7) Moulton, S. E.; Innis, P. C.; Kane-Maguire, L. A. P.; Ngamna, O.; Wallace, G. G. *Curr. Appl. Phys.* **2004**, *4*, 402.
(8) Stejskal, J.; Sapurina, I.; Trchová, M.; Proke×f0, J.; Køivka, I.; Tobolková, E. *Macromolecules* **1998**, *31*, 2218.
(9) Deore, B. A.; Hachey, S.; Freund, M. S. *Chem. Mater.* **2004**, *16*, 1427.
(10) Wang, H. L.; Gao, J.; Sansiñena, J. M.; McCarthy, P. *Chem. Mater.* **2002**, *14*, 2546.
(11) Huang, K.; Wan, M. *Chem. Mater.* **2002**, *14*, 3486.
(12) Zhang, L.; Wan, M. *J. Phys. Chem. B* **2003**, *107*, 6748.
(13) Zengin, H.; Zhou, W.; Jin, J.; Czerw, R., Jr.; Smith, D.; Echegoyen, L.; Carroll, D. L.; Foulger, S. H.; Ballato, J. *Adv. Mater.* **2002**, *14*, 1480.
(14) Master, W. K.; Benito, A. M.; Callejas, M. A.; Seeger, T.; Martínez, M. T.; Schreiber, J.; Muszynski, J.; Chauvet, O.; Osváth, Z.; Koós, A. A.; Biró, L. P. *Mater. Sci. Eng., C* **2003**, *23*, 87.
(15) Jia, W.; Tchoudakov, R.; Segal, E.; Narkis, M.; Siegmann, A. *J. Appl. Polym. Sci.* **2003**, *91*, 1329.
(16) Cho, M. S.; Choi, H. J.; Ahn, W. S. *Langmuir* **2004**, *20*, 202.
(17) Somani, P. R.; Marimuthu, R.; Mulik, U. P.; Sainkar, S. R.; Amalnerkar, D. P. *Synth. Met.* **1999**, *106*, 45.
(18) Ferreira, M.; Huguenin, F.; Zucolotto, V.; Silva, J. E. P.; Torresi, S. I. C.; Temperini, M. L. A.; Torresi, R. M., Jr.; Oliveira, O. N. *J. Phys. Chem. B* **2003**, *107*, 8351.
(19) Torres-Gómez, G.; Tejada-Rosales, E. M.; Gómez-Romero, P. *Chem. Mater.* **2001**, *13*, 3693.
(20) Zhou, Y. K.; He, B. L.; Zhou, W. J.; Huang, J.; Li, X. H.; Wu, B.; Li, H. L. *Electrochim. Acta* **2004**, *49*, 257.
(21) Kuwabata, S.; Takahashi, N.; Hirao, S.; Yoneyama, H. *Chem. Mater.* **1993**, *5*, 437.
(22) Frisch, H. L.; Song, H.; Ma, J.; Rafailovich, M.; Zhu, S.; Yang, N. L.; Yan, X. J. *Phys. Chem. B* **2001**, *105*, 11901.
(23) Zhang, Z.; Wan, M. *Synth. Met.* **2003**, *132*, 205.
(24) Lefenfeld, M.; Blanchet, G.; Rogers, J. A. *Adv. Mater.* **2003**, *15*, 1188.
(25) Huguenin.; Ferreira, M.; Zucolotto, V.; Nart, F. C.; Torresi, R. M.; Oliveira, O. N., Jr. *Chem. Mater.* **2004**, *16*, 2293.
(26) Tang, B. Z.; Geng, Y.; Lam, J. W. Y.; Li, B.; Jing, X.; Wang, X.; Wang, F.; Pakhomov, A. B.; Zhang, X. X. *Chem. Mater.* **1999**, *11*, 1581.
(27) Kovtyukhova, N. I.; Gorchinskiy, A. D.; Waraksa, C. *Mater. Sci. Eng.* **2000**, *B69−70*, 424.
(28) Michalak, F.; Aldebert, P. *Solid State Ionics* **1996**, *85*, 265.
(29) Zhang, X. W.; Wang, C.; Appleby, A. J.; Little, F. E. *J. Power Sources* **2002**, *109*, 136.
(30) Weimer, A. W. *Carbide, Nitride and Boride Materials*: *Synthesis and Processing*; Chapman & Hall: London, UK, 1997.
(31) Pearton, S. J.; Ren, F. *Adv. Mater.* **2000**, *12*, 1571.
(32) Aizawa, T.; Akhadejdamrong, T.; Iwamoto, C.; Ikuhara, Y.; Mitsuo, A. *J. Am. Ceram. Soc.* **2002**, *85*, 21.
(33) Janes, R. A.; Aldissi, M.; Kaner, R. B. *Chem. Mater.* **2003**, *15*, 4431.
(34) Kaskel, S.; Schlichte, K.; Chaplais, G.; Khanna, M. *J. Mater. Chem.* **2003**, *13*, 1496.
(35) Jiang, N.; Zhang, H. J.; Bao, S. N.; Shen, Y. G.; Zhou, Z. F. *Phys. B* **2004**, *352*, 118.
(36) (a) Li, J.; Gao, L.; Sun, J.; Zhang, Q.; Guo, J.; Yan, D. *J. Am. Ceram. Soc.* **2001**, *84*, 3045. (b) Zhang, Q. H.; Gao, L. *J. Eur. Ceram. Soc.* **2005**, in press, doi: 10.1016/j.jeurceramsoc.2005.03.243, JECS 5547 1-11.
(37) Kawano, S.; Takahashi, J.; Shimada, S. *J. Am. Ceram. Soc.* **2003**, *86*, 701.
(38) Xia, H.; Wang, Q. *Chem. Mater.* **2002**, *14*, 2158.
(39) Niu, Z.; Yang, Z.; Hu, Z.; Lu, Y.; Han, C. C. *Adv. Funct. Mater.* **2003**, *13*, 949.
(40) Müller, R.; Knapp, M.; Beckmann, K.; Ruthendorf, M. V.; Boden, G. *Langmuir* **2004**, *20*, 2598.
(41) Irvine, J. T. S.; Sinclair, D. C.; West, A. R. *Adv. Mater.* **1990**, *2*, 132.
(42) Khan, A. A.; Alam, M. M.; Mohammad, F. *Electrochim. Acta* **2003**, *48*, 2463.
(43) Lee, H. Y.; Kim, S. W.; Lee, H. Y. *Electrochem. Solid-State Lett.* **2001**, *4*, A19.
(44) Ryu, K. S.; Kim, K. M.; Kang, S. G.; Joo, J.; Chang, S. H. *J. Power Sources* **2000**, *88*, 197.